Published in final edited form as:

Heart Rhythm. 2019 September ; 16(9): 1383–1391. doi:10.1016/j.hrthm.2019.05.029.

Subcutaneous nerve stimulation for rate control in ambulatory dogs with persistent atrial fibrillation

Yuan Yuan, MD[1,2], **Xiao Liu, MD**[1], **Juyi Wan, MD**[1,3], **Johnson Wong, BS**[1], **Amanda A. Bedwell, MS**[4], **Scott A. Persohn, BA**[4], **Changyu Shen, PhD**[5], **Michael C. Fishbein, MD**[6], **Lan S. Chen, MD**[7], **Zhenhui Chen, PhD**[1], **Thomas H. Everett IV, PhD, FHRS**[1], **Paul R. Territo, PhD**[4], **Peng-Sheng Chen, MD, FHRS**[1]

[1.]The Krannert Institute of Cardiology and Division of Cardiology, Department of Medicine, Indiana University School of Medicine, Indianapolis, IN

[2.]Department of Cardiothoracic Surgery, Xinhua Hospital, Shanghai Jiaotong University School of Medicine, Shanghai, China

[3.]Department of Cardiothoracic Surgery, the Affiliated Hospital of Southwest Medical University, Luzhou, Sichuan Province , China

[4.]Department of Radiology and Imaging Sciences, Indiana University School of Medicine, Indianapolis, IN

[5.]Richard and Susan Smith Center for Outcomes Research in Cardiology, Beth Israel Deaconess Medical Center, Harvard Medical School, Boston, MA

[6.]The Department of Pathology and Laboratory Medicine, David Geffen School of Medicine at UCLA, Los Angeles, CA

[7.]Department of Neurology, Indiana University School of Medicine, Indianapolis, IN

Abstract

Background: Subcutaneous nerve stimulation (ScNS) damages the stellate ganglion and improves rhythm control of atrial fibrillation (AF) in ambulatory dogs.

Objective: To test the hypothesis that thoracic ScNS can improve rate control in persistent AF.

Methods: We created persistent AF in 13 dogs and randomly assigned them to ScNS (N=6) and sham control groups (N=7). ^{18}F-2-Fluoro-2-deoxyglucose (^{18}F-FDG) positron emission tomography / magnetic resonance imaging of the brain stem was performed at baseline and at the end of the study.

Corresponding Author: Peng-Sheng Chen, MD, 1800 N. Capitol Ave, E475, Indianapolis, IN 46202.

Disclosures

Johnson Wong and Thomas Everett have equity interest in Arrhythmotech, LLC. Other authors do not have conflicts.

Results: The average stellate ganglion nerve activity (aSGNA) reduced from 4.00±1.68 μV after the induction of persistent AF to 1.72±0.42 μV (p=0.032) after ScNS. In contrast, the aSGNA increased from 3.01±1.26 μV during AF to 5.52±2.69 μV after sham stimulation (p=0.023). The mean ventricular rate during persistent AF reduced from 149±36 bpm to 84±16 bpm (p=0.011) in ScNS group but no changes were observed in control. Left ventricular ejection fraction (LVEF) remained unchanged in ScNS group but reduced significantly in sham control group. Immunostaining showed damaged ganglion cells in bilateral stellate ganglia and increased brain stem glial cell reaction in the ScNS group but not in the controls. The ^{18}F-FDG uptake in pons and medulla was significantly (p=0.011) higher in the ScNS group than the sham control group at the end of the study.

Conclusions: Thoracic ScNS causes neural remodeling in the brain stem and stellate ganglia, controls the ventricular rate and preserves the LVEF in ambulatory dogs with persistent AF.

Keywords

Subcutaneous nerve stimulation; Autonomic nervous system; Neuromodulation; Persistent atrial fibrillation; Positron emission tomography; Magnetic resonance imaging

Introduction:

Both rhythm and rate controls are acceptable strategies in managing patients with atrial fibrillation (AF).[1, 2] Rapid ventricular rate (VR) may result in left ventricular dysfunction. Beta blockers are recommended by the current guidelines for both rate and rhythm control of AF.[2] While pharmacological agents are mostly effective in rate control of AF, atrioventricular nodal ablation may be needed in patients refractory to drug therapy.[2, 3] Alternative strategies of VR control include vagal nerve stimulation, which reduces the VR during AF in dogs.[4] Stimulating the auricular branch of the vagal nerve for one hour can suppresses AF and decreases inflammatory cytokines in patients with paroxysmal AF.[5] The acute effects of vagal nerve stimulation in those studies are attributed in part to parasympathetic activation. However, vagal nerve stimulation can also rapidly activate the stellate ganglion in ambulatory dogs probably through the activation of sympathetic nerve fibers within the vagal nerve.[6, 7] Rapid neuronal activation can cause neurotoxicity through intracellular calcium accumulation.[8, 9] Consistent with the latter observation, chronic intermittent vagal nerve stimulation can control the VR, reduce the stellate ganglion (SG) nerve activity (SGNA) and cause neurotoxicity in the SG.[10] If the effects of chronic vagal nerve stimulation are mediated through rapid excitation of the sympathetic nerve fibers within the vagal nerves, then it follows that stimulating any sympathetic nerve fibers connected to the SG may result in the same effects. The thoracic subcutaneous nerves in dogs originated primarily from the SG.[11] We recently showed that thoracic subcutaneous nerve stimulation (ScNS) from three different sites can rapidly activate the SG, suppress SGNA and result in rhythm control of atrial tachyarrhythmias in chronic canine models.[12, 13] The purpose of the present study was to test the hypothesis that ScNS can damage SG, reduce SGNA and control VR in ambulatory dogs with persistent AF.

Methods

The animal protocol was approved by the Institutional Animal Care and Use Committee of the Indiana University School of Medicine and the Methodist Research Institute, Indianapolis, IN, and conformed to the Guide for Care and Use of Laboratory animals.

Surgical procedures

Figure 1 shows the research protocol. Thirteen mongrel dogs (23-30 kg) underwent isoflurane inhalation general anesthesia and sterile left lateral thoracotomy through the forth intercostal space. A radiotransmitter (D70EEE, Data Sciences International, St. Paul, MN) was implanted to record SGNA and vagal nerve activity (VNA). A modified Medtronic Secura pacemaker (Medtronic Inc, Minneapolis, MN) was implanted during the same surgery for intermittent rapid atrial pacing through a pacing lead sutured onto the left atrial (LA) appendage. The skin incision was then extended to the back to reach left Xinshu acupoint (BL15, approximately 5 cm lateral to the spine at T5 level) as in a previous study.[12] The subcutaneous space was explored to locate visible subcutaneous nerves and blood vessels in that area. A Cyberonics Model 304 bipolar vagal stimulating lead was implanted around these small subcutaneous nerves and connected to a subcutaneously positioned Cyberonics Demipulse neurostimulator (Cyberonics Inc, Houston, TX) (Online supplement Figure 1). A third pair of the bipolar recording electrodes from the D70EEE radiotransmitter was placed in the subcutaneous tissue to record from the nerves being stimulated, with the two electrodes bracketing the point of stimulation. The latter bipolar leads have an interelectrode distance of > 4 cm. The chest was then closed.

Pacing protocol

The DSI radiotransmitter was turned on two weeks after surgery to record baseline rhythm and subcutaneous nerve activity (ScNA). After baseline recording, high-rate (600 beats/min, twice the diastolic threshold) atrial pacing was then initiated and continued for 2 weeks. The pacemaker was then turned off to determinate if there was persistent (>48 hours) of AF. If not, the atrial pacing was reinitiated until persistent AF was documented.

Subcutaneous nerve stimulation

After persistent AF was induced, the dogs were randomly assigned to ScNS group (N=6) and sham control group (N=7). The neurostimulator was turned on and programmed to 14-s ON and 1.1-min OFF (10 Hz, 500 μs pulse duration) based on the parameters used in a clinical trial.[14] The output current (mA) was progressively increased to 3.5 mA over 10 weeks. The dogs tolerated 3.5 mA stimulation without showing signs of discomfort or reduced appetite. After 10 weeks of ScNS, the stimulator was turned off for an additional 24 hours recording without ScNS. The sham control group underwent the same surgery, but the output current was set at 0 mA.

Functional imaging of brain stem

All dogs underwent brain stem ^{18}F-2-Fluoro-2-deoxyglucose (^{18}F-FDG) positron emission tomography (PET)–magnetic resonance imaging (MRI) for the functional survey before surgery (baseline). After 10 weeks of ScNS or sham stimulation, all implanted devices were

removed during a third sterile surgery. The dogs then underwent repeat PET/MRI imaging. A final PET/MRI imaging was performed after an additional 4-8 weeks of recovery. All PET/MRI images were imported and registered to their anatomical reference and baseline time point using a normalized entropy algorithm15 implemented in Analyze 11 (AnalyzeDirect, Stilwell KS). Fusion images were created between the registered PET and their respective MRI images. Image volumes were then manually segmented in 3D (Analyze 11; AnalyzeDirect, Stilwell KS) to obtain object maps for the pons and the medulla. Images were then quantified for amount of uptake in percent of injected dose per gram (%ID/g) within the region of interest in pons and medulla at baseline and follow up. A representative coronal slice was then exported and subjected to voxel-wise analysis to compute percentage change in %ID/g (Δ%ID/g) from baseline, and then mapped using custom developed software on anatomical MRI images yielding parametric maps which illustrate the changes in %ID/g.

Immunohistochemical Studies

After the dogs were euthanized, both SG were harvested and fixed in 4% formalin for 45-60 min, followed by storage in 70% alcohol for at least 48 hours. The tissues were processed routinely, paraffin embedded and cut into 5-μm thick sections. Immunohistochemical staining was performed with antibodies against tyrosine hydroxylase (TH) using mouse monoclonal anti-TH (Accurate Chemical, Westbury, NY). All slides were examined under a microscope to determine if there were regions of damage, characterized by decreased ganglionic cell density, pyknotic cell bodies, decreased TH staining, increased fibrosis and hypereosinophilia of neurons on Masson's trichrome staining. Digital photographs were taken from five roughly even spaced fields per slide with a 20× objective. The mean percentage of TH-negative ganglion cells was calculated manually in both SG using the same methods reported elsewhere. Terminal deoxynucleotidyl transferase dUTP nick end labeling (TUNEL) staining was performed to probe for cell death. A confocal microscope was used to detect TUNEL-positive cells. For quantitative analyses, we randomly selected 5 high power (40× objective) fields for image acquisition. We then manually counted the TUNEL-positive ganglion cells in each high power fields for analyses.

Data Analyses

The signals were manually analyzed using custom-written software to determine the temporal relationship between nerve activities and VR changes. Data from 3 recording electrodes were high-pass filtered at 150 Hz to obtain nerve activities, which were quantified by integrating the absolute value of the filtered signal over 20-s windows. The integrated nerve activities were then divided by the total number of samples (i.e., the product of sampling rate and 20) in each window to calculate the average SGNA (aSGNA), average vagal nerve activity (aVNA) and average subcutaneous nerve activity ScNA (aScNA). To quantify the hourly nerve activities over a 24-hr period, we selected for analyses 2-min of data at the beginning, 20 min, and 40 min past each hour when the stimulation was off. Artifacts or noises during that 2-min period were manually excluded from analyses. Nerve activities and VR were compared between different time points.

Statistical Analyses

The data were reported as mean ± Standard deviation (SD). Paired *t* tests were performed to compare the differences between HR, integrated nerve activities and the number of PAT episodes at different stages of experiments. Because paired *t* and signed rank reach similar p-values, only the paired *t* result is reported. The statistics were computed using the PASW Statistic (version 22; SPSS Inc, Chicago, IL). A two-sided p value of ≤0.05 was considered statistically significant.

Results

Effects of ScNS on nerve activities and ventricular rate during persistent AF

Figures 2A and 2B show the serial changes in the ratio of aSGNA and VR at different stages of the experiments in ScNS and sham control groups. Because the absolute values of aSGNA and VR vary among dogs, we used the ratio to baseline to display the relative changes during the course of the study. There was progressive reduction of aSGNA and VR in ScNS group but not in the sham control group. Compared to AF before ScNS, aSGNA was significantly reduced after 6 weeks of ScNS (p=0.045) and persisted afterwards. VR was significantly suppressed after 7 weeks of ScNS (p=0.011) and persisted afterwards. Asterisks indicate significant differences of aSGNA and VR between ScNS group and control group. Figure 2C and 2D show typical recordings of SGNA, VNA and ScNA at baseline and after the induction of AF, respectively. VNA and ScNA could either activate simultaneously (blue arrows) or at different times (asterisks) with SGNA. AF causes significant increase of SGNA. Figure 2E shows the acute effects of ScNS on SGNA. In that episode, SGNA was abruptly suppressed (red dot) followed by the progressive reduction of VR (black arrow).

Figures 3 shows a summary of all dogs studies. In ScNS group (Figure 3A), aSGNA was 4.00±1.68 μV immediately after induction of AF. The aSGNA then significantly reduced to 2.81±1.19 μV (p=0.030) at week 5 of stimulation, and persisted afterwards. In the final week of study, the aSGNA was 1.72±0.42 μV (p=0.011). Figure 3B shows the data in sham control group. aSGNA was 4.23±1.48 μV after the induction of AF. Weekly analyses showed non-significant increase of aSGNA to 4.72±0.95 μV at week 5 (p=0.229) and to 5.90±2.20 μV at the final week of study (p=0.072). The mean VR was 149±36 bpm after the induction of AF. The VR significantly decreased to 84±16 bpm (p=0.011) at the final week of ScNS. Figure 3B shows in sham control group, the mean VR was 170±33 bpm after the induction of AF. At the final week of monitoring, the mean VR of sham control group reduced insignificantly to 153±25 bpm (p=0.262), which was significantly higher than the final VR of the ScNS group (p<0.001). The aVNA and aScNA did not change significantly during the study in either group. Figure 4 shows examples of 24-hr SGNA at baseline sinus rhythm, after AF induced and after either 3.5 mA or sham (0 mA) ScNA in the ScNS group (A) and in the sham control group (B). SGNA was significantly increased after persistent AF in both groups. Compared to AF, SGNA was suppressed after ScNS (Figure 4A), but did not change in the sham control group (Figure 4B).

Prolonged pauses during persistent AF

Prolonged (>3s) pauses were observed with increased frequency in the ScNS group but not in the sham control group. Figure 5A shows SGNA is associated with VR acceleration during AF (arrow). Prolonged pauses (asterisks) happened frequently after ScNS in the absence of SGNA bursts. The average number of prolonged pauses after the induction of persistent AF (but before ScNS) was similar in the ScNS group (5±4 episodes/d) and in the sham control group (5±7/d, p=0.93). After completing the ScNS protocol, the number of prolonged paused was 38±19/d in the ScNS group and 10±8 times in the sham control group (p=0.028).

The left ventricular ejection fraction (LVEF) was 68±2% in the ScNS group and 69±3% in the sham control group during baseline sinus rhythm (p=0.823). After the induction of persistent AF and completing the ScNS protocols, LVEF was 68±4% in the ScNS group, significantly higher than that in the sham control group (55±3%, p<0.001) (Figure 5C).

SG remodeling after ScNS in persistent AF dogs

Bilateral SG were successfully harvested for histology analyses. The SG from the ScNS group showed large damaged regions (Figure 6A and 6C). Multiple ganglion cells in damaged regions showed pyknotic nuclei, contracted and hypereosinophilic cytoplasm in the Masson trichrome stained sections. The damaged regions could be either confluent or multifocal. These changes were not observed in SG from the sham control group. TH staining showed abundant of TH-negative ganglion cells in the damaged regions of the ScNS group. Within the damaged region, the percentage of TH-negative ganglion cells was 28.89±15.22% in the left SG and 26.56±22.13% in the right SG in the ScNS group, which were significantly higher than that of the sham control group (6.40±10.04%, p=0.013 and 4.02±5.41%, p=0.036, respectively).

Brain stem remodeling

Figure 7A (Sham control group) and 7B (ScNS group) from left to right show 3T T2W SPACE3D MRI, ^{18}F-FDG PET, PET/MRI Fused, and percent changes from baseline. The rows from top to bottom show the images obtained at baseline, after ScNS and after recovery, respectively. Blinded volumetric analyses showed ^{18}F-FDG uptake in pons and medulla of the sham control group had no statistically significant time-dependent changes. In contrast, ^{18}F-FDG uptake in pons and medulla of the ScNS group of dogs continued to increase (Figure 7C). The mean Δ%ID/g in the pons of the ScNS group went from 14.84% to 13.54% and in the medulla 15.64% to 18.22%. In the sham control group the mean Δ %ID/g went from 3.92% to −5.07% in pons and 5.27% to −6.07%. The final differences in ^{18}F-FDG uptake between these two groups were statistically significant (p=0.011, Figure 7D).

All brain stems were successfully harvested for histology analyses. Figure 8A shows the GFAP staining of the brain stem from the ScNS group (a and b) and from the sham control group (c and d). Brown color indicates the GFAP-positive glial cells. The densities of GFAP immunoreactivity were significantly higher in the ScNS group (32700±12900 $\mu m^2/mm^2$) than that in the sham control group (16900±7300 $\mu m^2/mm^2$, p=0.026). Figure 8B shows

terminal deoxynucleotidyl transferase dUTP nick end labeling (TUNEL) staining with GFAP double immunofluorescence staining. The red colors shows positive GFAP staining while the green color is expected for TUNEL positive cells. There were more GFAP activity in the ScNS group (a and b) than in the sham control group (c and d). No TUNEL-positive neuron cells were observed in either group.

Discussion

We found that ScNS reduces VR and aSGNA but increases the frequencies of long pauses during persistent AF. These changes are associated with significant brain stem and SG remodeling.

Neural Remodeling

Electrical stimulation is a commonly used method for managing human diseases, including cardiac arrhythmias.[15] Because the autonomic nervous system is highly plastic, chronic electrical stimulation is likely to result in significant neural remodeling. Chronic stimulation of the vagal nerves and the subcutaneous tissues can be associated with significant remodeling of the SG.[10, 12, 16] Electrical stimulation applied to the left cymba conchae could produce significant activation of the classical central vagal projections in functional magnetic resonance imaging.[17] Like that found in the present study, the SG changes include increased percentage of TH-negative cells and TUNEL-positive neurons. Radiofrequency catheter ablation of the renal sympathetic nerves is associated with similar changes in the SG.[18] However, contrary to that found in dogs underwent renal denervation, we found that the ^{18}F-FDG uptake in the brain stem is increased. While there are significant glial cell reactions, there are no TUNEL-positive cells in the brain stem. The combined use of PET and MRI for functional studies of the brain has undergone significant evolution in recent years.[19] The glucose analog ^{18}F-FDG is a surrogate marker for glucose metabolism that is generally increased in malignant tumors and inflammation. Because neuronal activity is dependent upon glucose metabolism,[20] the findings in this study suggest that there is increased brain stem activity in dogs with ScNS as compared with sham controls. Viral transneuronal labeling studies have found that brain stem is connected with the sympathetic preganglionic neurons at the lateral horn, which project to the SG.[21] It is possible that the SG remodeling could lead to brain stem remodeling through these direct connections.

ScNS versus drug therapy for ventricular rate control

Dosdall et al[22] reported that a combination of digoxin and metoprolol can reduce the average ventricular rate in canine pacing-induced chronic AF from 172 bpm to 130 bpm after 6 months, along with a reduction of LVEF from 54% to 33%. In comparison, we showed that ScNS reduced the VR from 149 bpm to 84 bpm in 6 weeks with no change of LVEF. These findings suggest that ScNS may be more effective than drug therapy in controlling ventricular rate. However, due to shorter duration of follow up, whether or not ScNS can preserve LVEF after 6 months of AF remains unclear.

Clinical implications

Ventricular rate control is an important strategy in managing patients with AF.[1] When drug therapy fails to achieve rate control, nonpharmacological therapy such as catheter ablation of the atrioventricular node may be needed. ScNS may provide an alternative to atrioventricular node ablation. Instead of using subcutaneously implanted electrodes, it is also possible that transcutaneous electrical nerve stimulation can achieve similar therapeutic effects. However, we do not have data to test that hypothesis.

Similar to chronic vagal nerve stimulation,[10] chronic ScNS can increase the frequencies of long pauses during AF. These iatrogenic long (> 3 s) pauses may lead to a need for pacemaker insertions.[23] Our recent studies[24] showed that the strength of electrical stimulation is important in determining the electrophysiological responses. Very low dose (0.25 mA) increases serum norepinephrine, causes nerve sprouting and is proarrhythmic. Intermediate dose (2.5 mA) do not increase norepinephrine levels and appears to be similarly antiarrhythmic as 3.5 mA. In that study, the dogs were in sinus rhythm. Whether or not the data are applicable to rate control of AF remains unclear. If there is a future clinical trial on ScNS or TENS in AF rate control, the relationship between stimulation strength and the bradycardic complications will need to be carefully considered.

Limitations

The study duration is insufficient to determine the persistent efficacy or the reversibility of the neural remodeling induced by ScNS.

Supplementary Material

Refer to Web version on PubMed Central for supplementary material.

Acknowledgement

We thank Nicole Courtney, Christopher Corr and David Adams for their assistance.

Source of Funding

This study was supported by NIH Grants R42DA043391, TR002208-01, R01 HL139829, R56HL71140, American Heart Association Grant #18TPA34170284 /ZC/2018a, a Medtronic-Zipes Endowment of the Indiana University and the Indiana University Health-Indiana University School of Medicine Strategic Research Initiative.

References

1. Wyse DG, Waldo AL, DiMarco JP, et al. A comparison of rate control and rhythm control in patients with atrial fibrillation. N.Engl.J.Med 2002;347:1825–1833. [PubMed: 12466506]
2. January CT, Wann LS, Alpert JS, et al. 2014 AHA/ACC/HRS guideline for the management of patients with atrial fibrillation: a report of the American College of Cardiology/American Heart Association Task Force on Practice Guidelines and the Heart Rhythm Society. J Am Coll Cardiol. 2014;64:e1–76. [PubMed: 24685669]
3. Ozcan C, Jahangir A, Friedman PA, et al. Long-term survival after ablation of the atrioventricular node and implantation of a permanent pacemaker in patients with atrial fibrillation. N Engl J Med. 2001;344:1043–1051. [PubMed: 11287974]

4. Zhuang S, Zhang Y, Mowrey KA, et al. Ventricular rate control by selective vagal stimulation is superior to rhythm regularization by atrioventricular nodal ablation and pacing during atrial fibrillation. Circulation. 2002;106:1853–1858. [PubMed: 12356641]
5. Stavrakis S, Humphrey MB, Scherlag BJ, et al. Low-level transcutaneous electrical vagus nerve stimulation suppresses atrial fibrillation. J Am Coll Cardiol. 2015;65:867–875. [PubMed: 25744003]
6. Rhee KS, Hsueh CH, Hellyer JA, et al. Cervical vagal nerve stimulation activates the stellate ganglion in ambulatory dogs. Korean Circ J. 2015;45:149–157. [PubMed: 25810737]
7. Onkka P, Maskoun W, Rhee KS, et al. Sympathetic nerve fibers and ganglia in canine cervical vagus nerves: Localization and quantitation. Heart Rhythm. 2013;10:585–591. [PubMed: 23246597]
8. Olney JW, deGubareff T, Sloviter RS. "Epileptic" brain damage in rats induced by sustained electrical stimulation of the perforant path. II. Ultrastructural analysis of acute hippocampal pathology. Brain Res Bull. 1983;10:699–712. [PubMed: 6871738]
9. Olney JW. Excitotoxicity, apoptosis and neuropsychiatric disorders. Curr Opin Pharmacol. 2003;3:101–109. [PubMed: 12550750]
10. Chinda K, Tsai WC, Chan YH, et al. Intermittent Left Cervical Vagal Nerve Stimulation Damages the Stellate Ganglia and Reduces Ventricular Rate During Sustained Atrial Fibrillation in Ambulatory Dogs. Heart Rhythm. 2016;13:771–780. [PubMed: 26607063]
11. Taniguchi T, Morimoto M, Taniguchi Y, Takasaki M, Totoki T. Cutaneous distribution of sympathetic postganglionic fibers from stellate ganglion: A retrograde axonal tracing study using wheat germ agglutinin conjugated with horseradish peroxidase. J Anesth. 1994;8:441–449. [PubMed: 28921353]
12. Yuan Y, Jiang Z, Zhao Y, et al. Long-term intermittent high-amplitude subcutaneous nerve stimulation reduces sympathetic tone in ambulatory dogs. Heart Rhythm. 2018;15:451–459. [PubMed: 29081397]
13. Zhao Y, Yuan Y, Tsai WC, et al. Antiarrhythmic effects of stimulating the left dorsal branch of the thoracic nerve in a canine model of paroxysmal atrial tachyarrhythmias. Heart Rhythm. 2018;15:1242–1251. [PubMed: 29654853]
14. Dicarlo L, Libbus I, Amurthur B, Kenknight BH, Anand IS. Autonomic regulation therapy for the improvement of left ventricular function and heart failure symptoms: the ANTHEM-HF study. J Card Fail. 2013;19:655–660. [PubMed: 24054343]
15. Chen PS, Chen LS, Fishbein MC, Lin SF, Nattel S. Role of the autonomic nervous system in atrial fibrillation: pathophysiology and therapy. Circ Res. 2014;114:1500–1515. [PubMed: 24763467]
16. Shen MJ, Hao-Che Chang X, Park HW, et al. Low-level vagus nerve stimulation upregulates small conductance calcium-activated potassium channels in the stellate ganglion. Heart Rhythm. 2013;10:910–915. [PubMed: 23357541]
17. Frangos E, Ellrich J, Komisaruk BR. Non-invasive Access to the Vagus Nerve Central Projections via Electrical Stimulation of the External Ear: fMRI Evidence in Humans. Brain Stimul. 2015;8:624–636. [PubMed: 25573069]
18. Tsai W-C, Chan YH, Chinda K, et al. Effects of renal sympathetic denervation on the stellate ganglion and the brain stem in dogs. Heart Rhythm. 2017;14:255–262. [PubMed: 27720832]
19. Broski SM, Goenka AH, Kemp BJ, Johnson GB. Clinical PET/MRI: 2018 Update. AJR Am JRoentgenol. 2018;211:295–313. [PubMed: 29949413]
20. Barros LF, Deitmer JW. Glucose and lactate supply to the synapse. Brain Res Rev. 2010;63:149–159. [PubMed: 19879896]
21. Jansen ASP, Wessendorf MW, Loewy AD. Transneuronal labeling of CNS neuropeptide and monoamine neurons after pseudorabies virus injections into the stellate ganglion. Brain Res. 1995;683:1–24. [PubMed: 7552333]
22. Dosdall DJ, Ranjan R, Higuchi K, et al. Chronic atrial fibrillation causes left ventricular dysfunction in dogs but not goats: experience with dogs, goats, and pigs. Am J Physiol Heart Circ Physiol. 2013;305:H725–731. [PubMed: 23812387]
23. Epstein AE, Dimarco JP, Ellenbogen KA, et al. ACC/AHA/HRS 2008 guidelines for Device-Based Therapy of Cardiac Rhythm Abnormalities: executive summary. Heart Rhythm. 2008;5:934–955. [PubMed: 18534377]

24. Wan J, Chen M, Yuan Y, et al. Antiarrhythmic and proarrhythmic effects of subcutaneous nerve stimulation in ambulatory dogs. Heart Rhythm. 2019:pii: S1547-5271(1519)30149-30143. doi: 30110.31016/j.hrthm.32019.30102.30027. [Epub ahead of print].

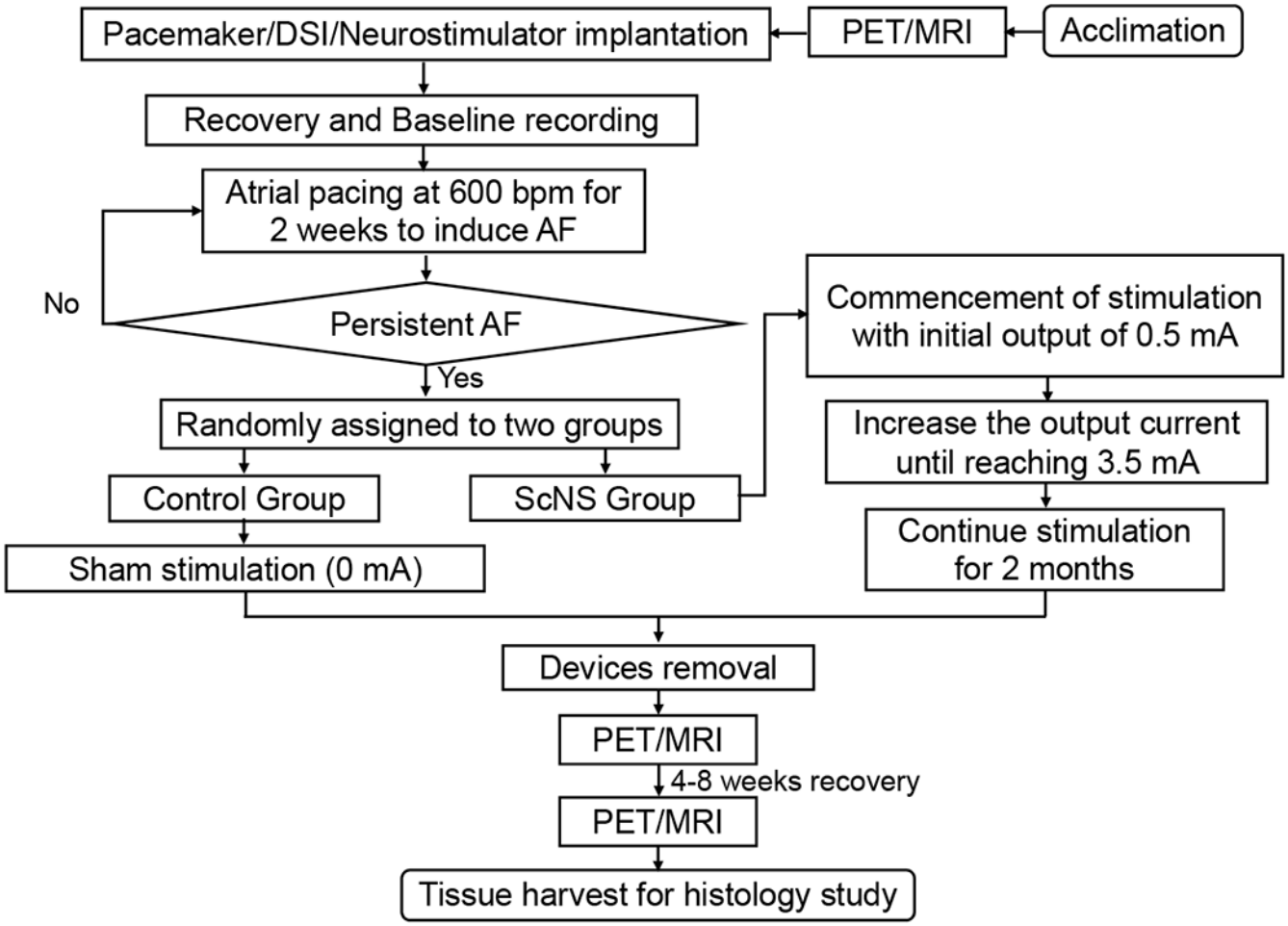

Figure 1.

Schematic of the study protocol. The first ^{18}F-FDG PET/MRI was performed before surgery. The baseline nerve activity and ECG were recorded two weeks after radiotransmitter implantation. After persistent AF was induced, the dogs were randomly assigned to thoracic subcutaneous nerve stimulation (ScNS) and sham control group.

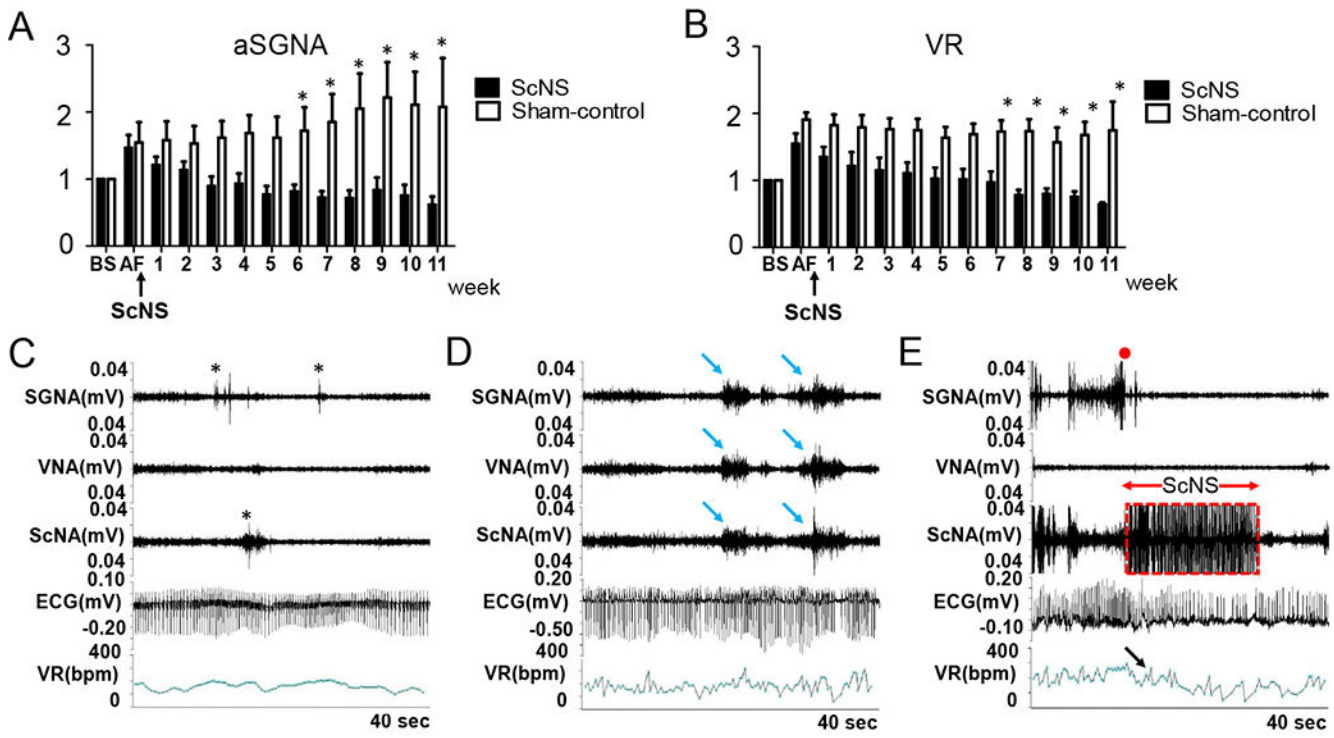

Figure 2.

Effects of ScNS on SGNA, VR, VNA and ScNA. The serial changes in the ratio of average SGNA (**A**) and VR (**B**) at different times after persistent AF in the ScNS group (filled columns) and in the sham control group (unfilled columns). In comparison with baseline, there are significant decreases in aSGNA after 6 weeks and in VR after 7 weeks of ScNS. **C:** Examples of baseline nerve discharges (asterisks). **D:** SGNA, VNA and ScNA co-firing (blue arrow) discharges during persistent AF. **E:** Abrupt (red dot) reduction of SGNA during ScNS ON-time (box) after 10 weeks of ScNS, which is associated with a reduction of VR (black arrow). Asterisks indicate significant differences of aSGNA and VR between ScNS group and control group.

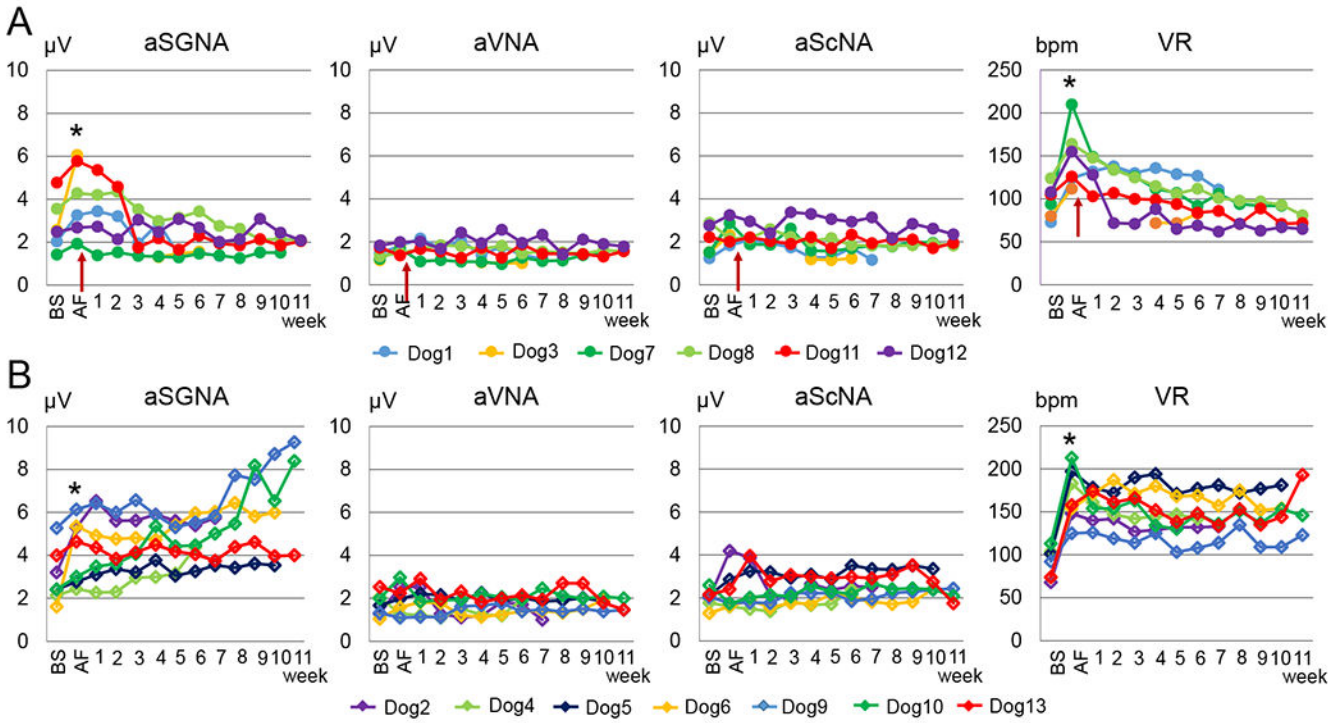

Figure 3.

Changes of nerve activities and VR in ScNS group and in sham control group. **A:** aSGNA increased after persistent AF and reduced gradually after ScNS (red arrow) in ScNS group. The reduction was statistically significant compared to baseline after 4 or more weeks of ScNS. Ventricular rate significantly increased after persistent AF and gradually reduced after ScNS onset (red arrow). Average VNA (aVNA) and average ScNA (aScNA) did not change significantly by ScNS. **B:** aSGNA increased after persistent AF and kept increasing in the following weeks in sham control group. Ventricular rate increased significantly after persistent AF and then fluctuated but did not show a stable trend of increase or decrease.

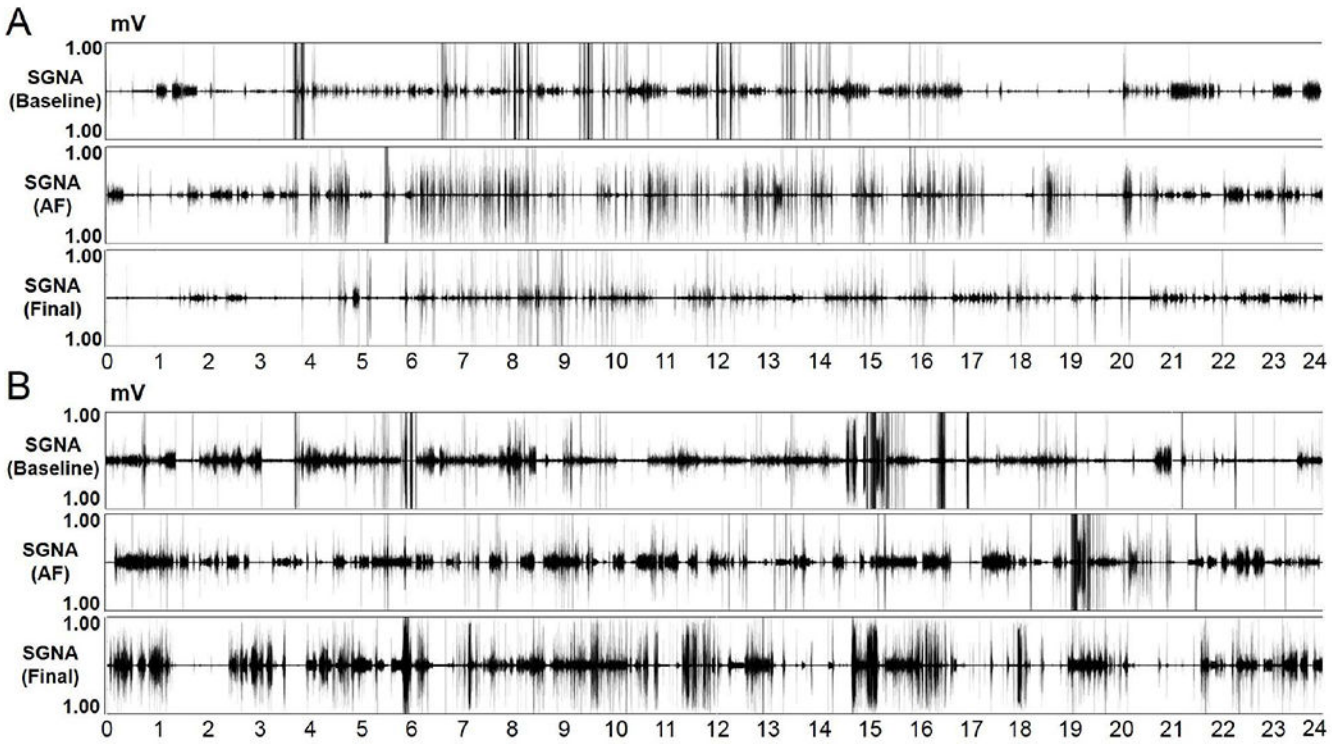

Figure 4.

Nerve activity over a 24-hr period. **A:** SGNA at baseline (upper panel), during persistent AF (middle panel) and after 11 weeks of ScNS (lower panel) in the ScNS group. **B:** SGNA at baseline (upper panel), during persistent AF (middle panel) and after 11 weeks of follow up (lower panel) in sham control group.

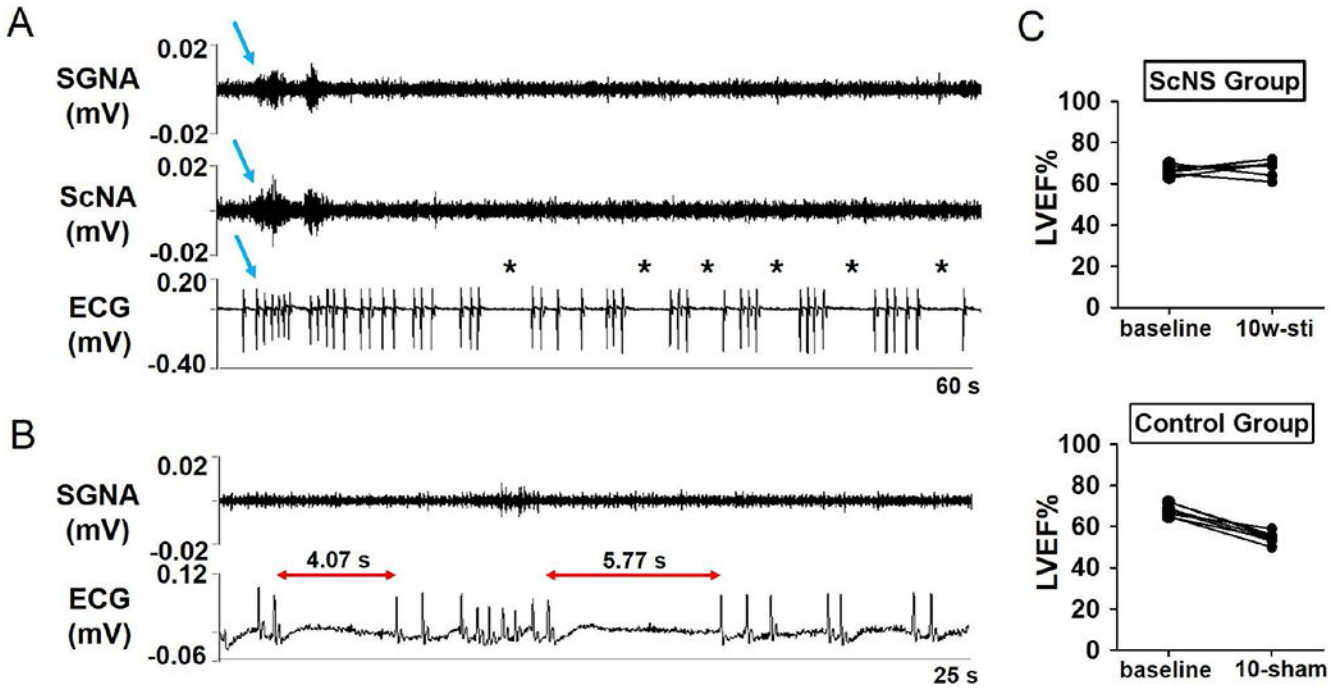

Figure 5.

Long pauses (>3s) induced by ScNS. **A** shows SGNA associated with VR acceleration during AF (blue arrow). When SGNA was quiescent, the RR-interval lengthened. Six episodes of long pauses were observed (asterisks) in the 60-s period. **B** shows the longest pause (5.77 s) found in this study from a dog with ScNS. C shows LVEF changes in ScNS group (upper panel) and sham control group (lower panel). LVEF decreased significantly after persistent AF in sham control group but not in ScNS group.

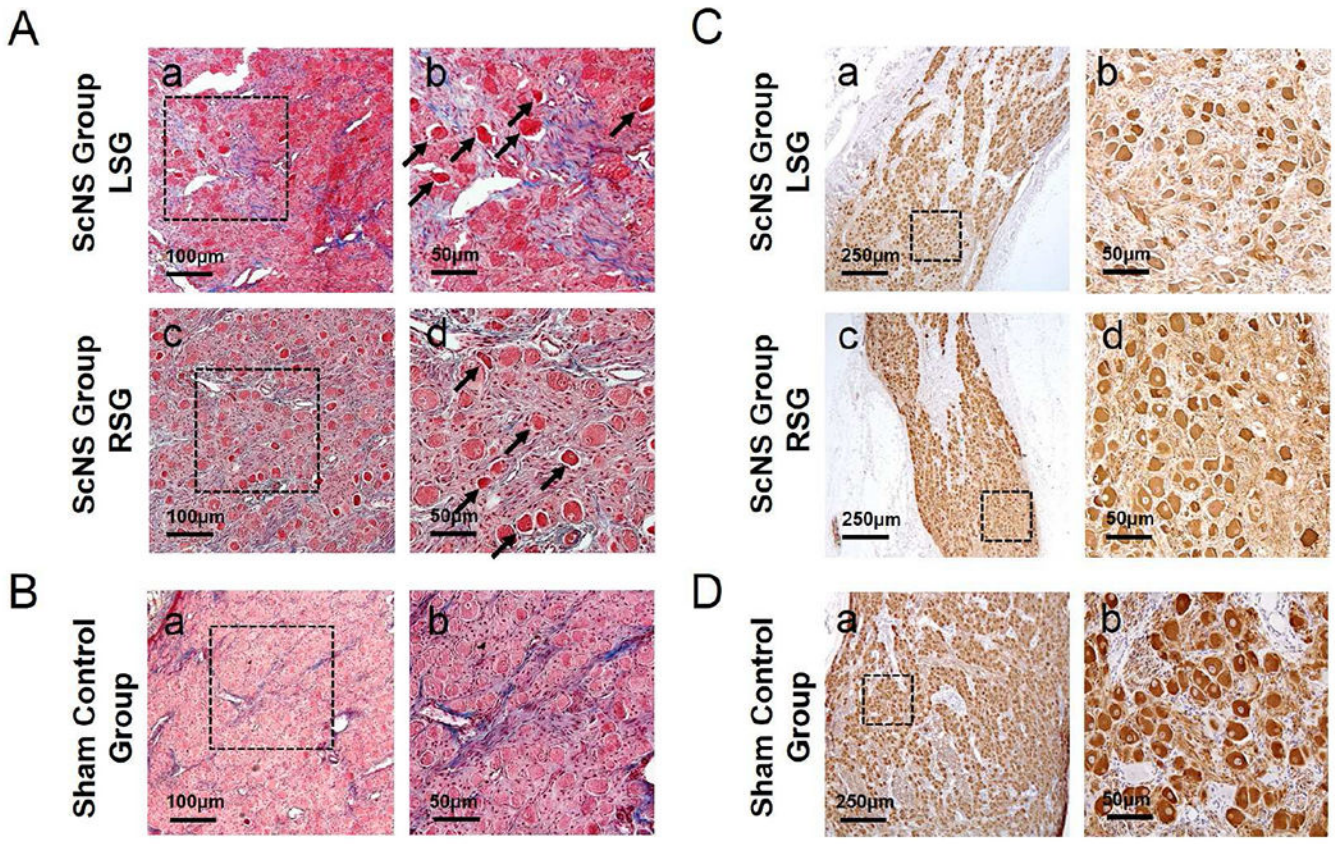

Figure 6.

Typical examples of Masson's trichrome staining and tyrosine hydroxylase (TH) staining in SGs after ScNS. **A:** Masson's trichrome staining in ScNS group shows the presence of damaged region with increased fibrosis in both left SG (LSG) (**a**) and right SG (RSG) (**c**). (Calibration bar=100 μm). High power view of the damaged regions show increased abnormal morphology of damaged neurons with eosinophilic staining (**b** and **d**, arrows). (Calibration bar=50 μm). **B:** Masson's trichrome staining shows normal neurons in the sham control group.**C:** TH staining showed the reduced TH staining in damaged region in both LSG (**a**) and RSG (**c**) in ScNS group. (Calibration bar=250 μm). High power view shows the neurons in the damaged region appeared small and had pyknotic nuclei (**b** and **d**). Many neurons stained negatively or weakly for TH (arrow). (Calibration bar=50 μm). **D:** TH staining showed normal morphology and positive TH-stained neurons in sham control group.

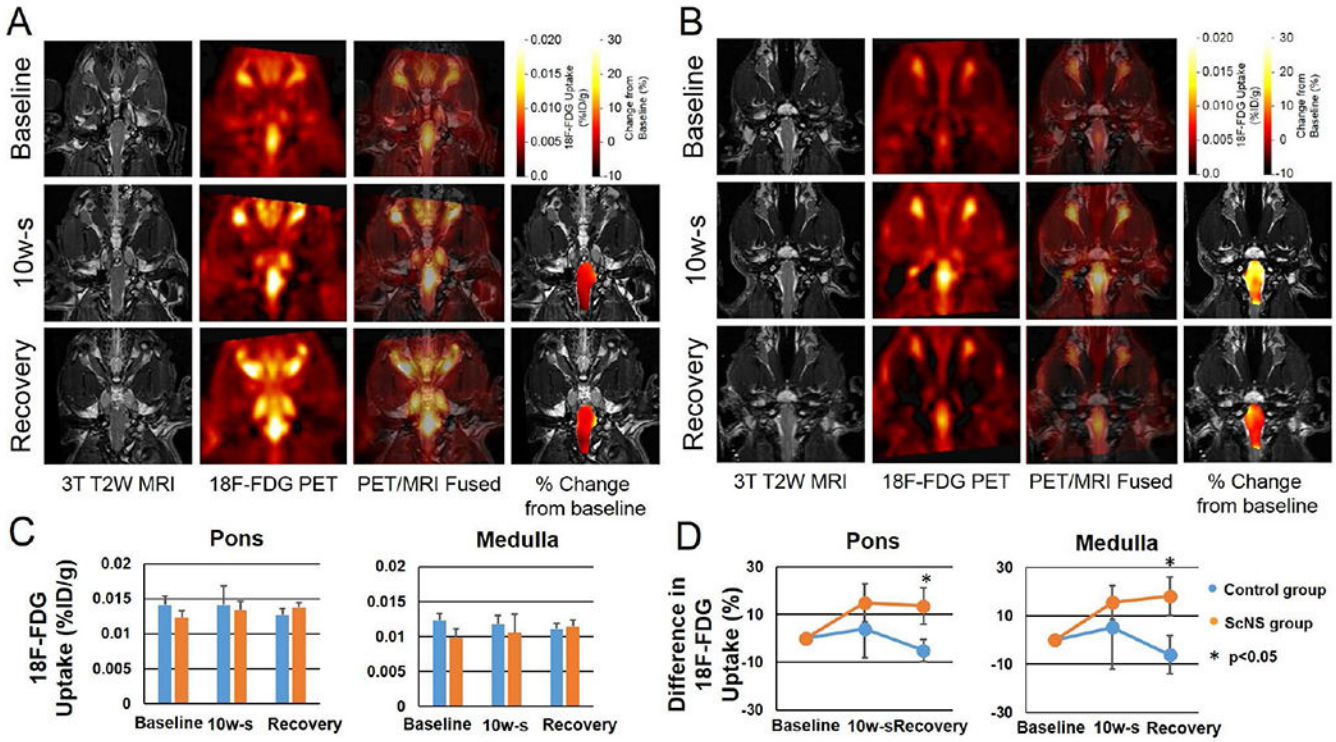

Figure 7.

Functional imaging of brain stem in ScNS group and sham control group. **A** (sham control group) and **B** (ScNS group) from left to right show 3T T2W SPACE3D MRI, ^{18}F-2-Fluoro-2-deoxyglucose (^{18}F-FDG), PET/MRI Fused, and percent changes from baseline. The rows from top to bottom show the images obtained at baseline, after ScNS and after recovery, respectively. Blinded volumetric analyses showed ^{18}F-FDG uptake in pons and medulla of the sham control group had no statistically significant time-dependent changes. In contract, ^{18}F-FDG uptake in pons and medulla of ScNS group dogs continued to increase (**C**). After 4-8 weeks of recovery, the final differences in ^{18}F-FDG uptake between these two groups were statistically significant (**D**).

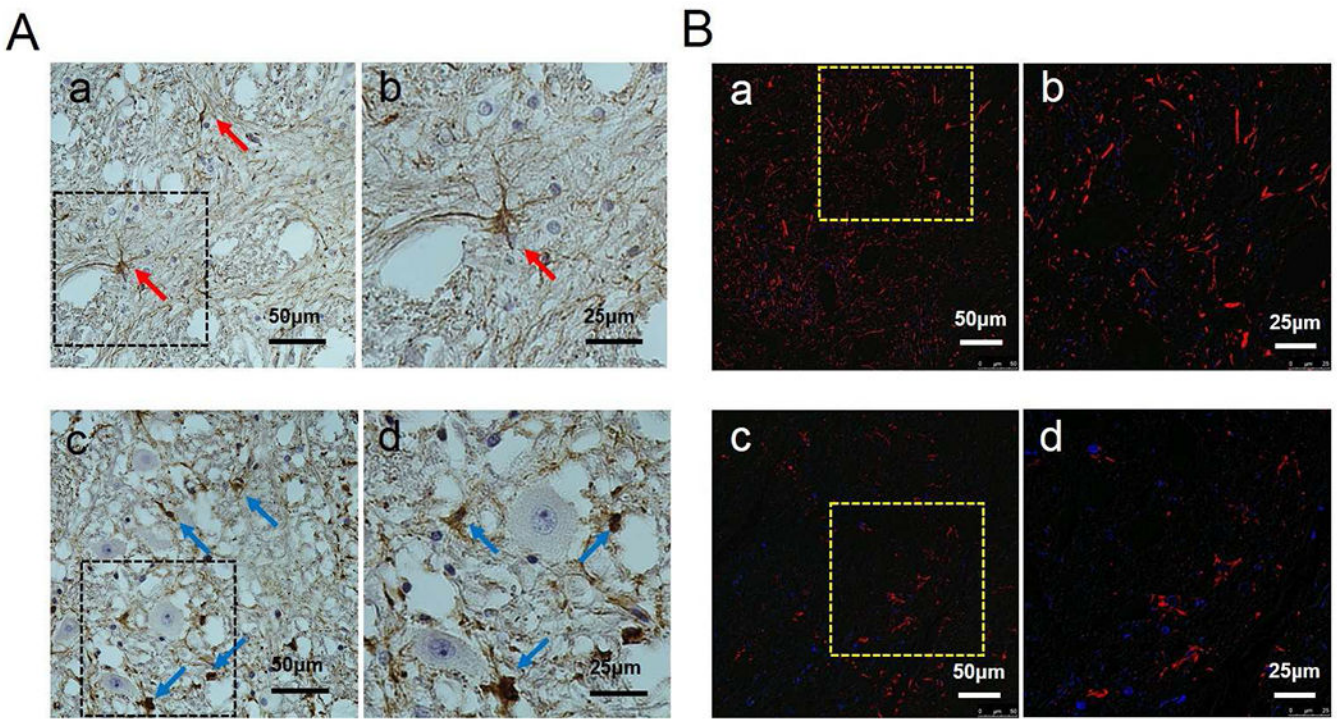

Figure 8.

Histology results of brain stem show difference in ScNS group and sham control group. **A:** Immunostaining of glial fibrillary acidic protein (GFAP) shows strong glial cell reaction in the brain stem of the ScNS group (**a** and **b**. red arrow), but not in the sham control group (**c** and **d**, blue arrow). **B:** Confocal microscope images of immunofluorescent GFAP (red) and terminal deoxynucleotidyl transferase dUTP nick end labeling (TUNEL, green) show no TUNEL-positive neuro cells in either ScNS group (**a** and **b**) or sham control group (**c** and **d**). Blue is the DAPI stain of the nuclei.